Versatile approximation of the lung field boundaries in chest radiographs in the presence of bacterial pulmonary infections

Dimitris K. Iakovidis, *Member, IEEE*

***Abstract*—The most common radiographic manifestation of bacterial pulmonary infections are foci of consolidation which are visible as bright shadows interfering with the interior lung intensity. In critically-ill patients this interference can be severe leading to vague or invisible lung field boundaries which are difficultly distinguished even by experienced physicians. This problem is amplified if the radiographs are of low quality as obtained with a portable x-ray device, routinely used in intensive care units. This paper proposes a pioneering methodology that copes with lung field detection in both stationary and portable chest radiographs by combining statistical grey-level intensity information and directional edge maps. The boundaries of the lung fields are approximated by consecutive intuitively manipulated parametric curves. Conventional and state of the art lung field detection approaches address only stationary radiography, and only a few of them cope with pulmonary infections. The proposed methodology features unsupervised operation, it is not iterative, it is not limited by the patients' positioning, and it is tolerant to the presence of consolidations and boundary discontinuities of the lung fields. Its performance is validated on various stationary radiographs and on a set of portable radiographs obtained from patients with bacterial pulmonary infections.**

I. Introduction

Detection of the lung fields is usually the first and most critical step in computerized analysis of chest radiographs. Once the boundaries of the lung fields are known, further assessment of the condition of the lungs can take place.

The first approaches to lung field detection begun to appear in the early sixties [1]. Since then, a variety of approaches have been proposed for automatic detection of the lung fields and approximation of their boundaries. The most popular methods rely on rules on the locations and on the intensity profiles of the anatomic structures in conjunction with image processing techniques such as contrast enhancement, edge detection, merging and splitting operations [6]-[10]. Other methods include machine learning algorithms [11]-[13], active shape models [14]-[17], and graph cuts [18].

Most of the afore-mentioned methodologies have mainly been evaluated on radiographs of normal or minimally distorted lungs. Robustness against the presence of abnormalities that interfere with interior lung intensity has been demonstrated in [5],[15] using active shape models, and in [18] using graph cuts. However, the former are supervised, therefore they depend on the selection of a representative training dataset, whereas none of these studies provide or mention results from their application on diseased lungs with severe intensity distortions visible in the chest radiograph.

This paper accepts the challenge to cope with automatic detection of the lung fields and approximation of their boundaries, even in severe cases of bacterial pulmonary infections. The most common radiographic manifestation of such infections are foci of consolidations, visible as bright shadows interfering with the interior lung intensity [2]. In critically-ill patients this interference can be severe leading to vague or invisible lung field boundaries which are difficultly distinguished even by experienced physicians [3].

Another important issue arising with the analysis of chest radiographs obtained from critically-ill patients is that most of them are acquired with a portable x-ray device in an uncontrolled environment. This is an unavoidable consequence as the patients are usually in pain and immobilized in bed. Therefore, portable radiographs are usually of low quality mainly due to misaligned body positioning during acquisition [3]. This fact introduces an additional degree of difficulty in their interpretation, subjecting to a higher misinterpretation rate.

The proposed methodology is versatile, in the sense that it copes with lung field detection in both stationary and portable chest radiographs by combining statistical grey-level intensity information and directional edge maps. The boundaries of the lung fields are approximated by consecutive intuitively manipulated parametric curves. In contrast to the supervised state of the art methodologies [5],[15], it features unsupervised operation, it is not limited by patients' positioning as most other rule-based approaches do [6]-[10] and unlike edge-based methods [18] it is tolerant to boundary discontinuities which may arise from severe consolidations or low image quality.

The rest of this paper comprises of three sections. The proposed methodology is described in Section II. Section III presents the results of its experimental evaluation on a variety of radiographs from various sources, and the last section summarizes the conclusions of this study.

Manuscript received July 5, 2008. This work was supported in part by the European Commission's Seventh Framework Information Society Technologies (IST) Programme, Unit ICT for Health, project DEBUGIT (no. 217139).

D. K. Iakovidis is with the Technological Educational Institute of Lamia, Dept. of Informatics and Computer Technology, GR-35100 Lamia, Greece (e-mail: dimitris.iakovidis@ieee.org).

II. Methodology

Let I be a chest radiograph of size $N \times M$ pixels. Considering the case that the radiograph may have been obtained from a patient immobilized in bed, possibly in a skewed position, the proposed methodology assumes that the patient's body may not necessarily be aligned with the x-ray device. The lung field boundaries are determined using feature points efficiently detected on the surrounding anatomic structures, which remain unaffected by the presence of pulmonary bacterial infections. The feature points are then purified by a simple outlier removal mechanism, and used to control a parametric curve that approximates the lung field boundaries.

A. Feature point detection

Feature point detection is based on both statistical grey-level intensity information extracted from the radiographic opacities and directional edge maps derived from I. As a first step the radiographic image is normalized to enhance the contrast of the visible anatomic structures. In the sequel, feature points are detected at the outer, the inner and the bottom boundaries of the lung fields.

1) Spinal cord detection and feature points of the outer left and right lung field boundaries: The spinal cord and the bones of the ribcage are the densest structures visible in a chest radiograph [20]. Consequently they are mainly characterized by higher grey-level intensities than the other anatomic structures. The outer left and right lung field boundaries are defined by the ribcage sideways.

In order to detect feature points on the spinal cord and on the ribcage sideways, radiograph I is uniformly sampled from top to bottom with s_h non-overlapping rectangular windows of $h \times M$, pixels, where $h<N$. For each sample an average horizontal profile, i.e. the average grey-level of its rows, per column, is estimated. Radiographic image profiles have been proved valuable in several radiographic image analysis tasks [1],[4],[6],[7],[10] as they provide a simple though effective means to navigating through a radiograph by using only one-dimensional information and elementary signal processing techniques. The proposed methodology utilizes horizontal profiles of subsequent image samples in order to obtain spatial instances of the radiograph from which the spinal cord and the ribcage boundaries are detectable even if the patient is bent. Figure 1(c) illustrates six of the nineteen profiles corresponding to the horizontal samples illustrated in Fig. 1(b). It can be easily noticed that the central peaks visible in profiles 1-16 correspond to the spinal cord. The two valleys around the central peak in profiles 4-16 correspond to the lung fields, whereas the peaks after these valleys correspond to the ribcage boundaries. Each profile is smoothed by following a moving average approach that facilitates noise insensitivity. The local maxima detected for each profile are illustrated as white points in Fig. 1(b). The localization of the maxima remains practically unaffected by the presence of consolidations, since their density, and therefore their grey-level intensity, is generally lower than the density of the spinal cord and of the ribcage [1],[20].

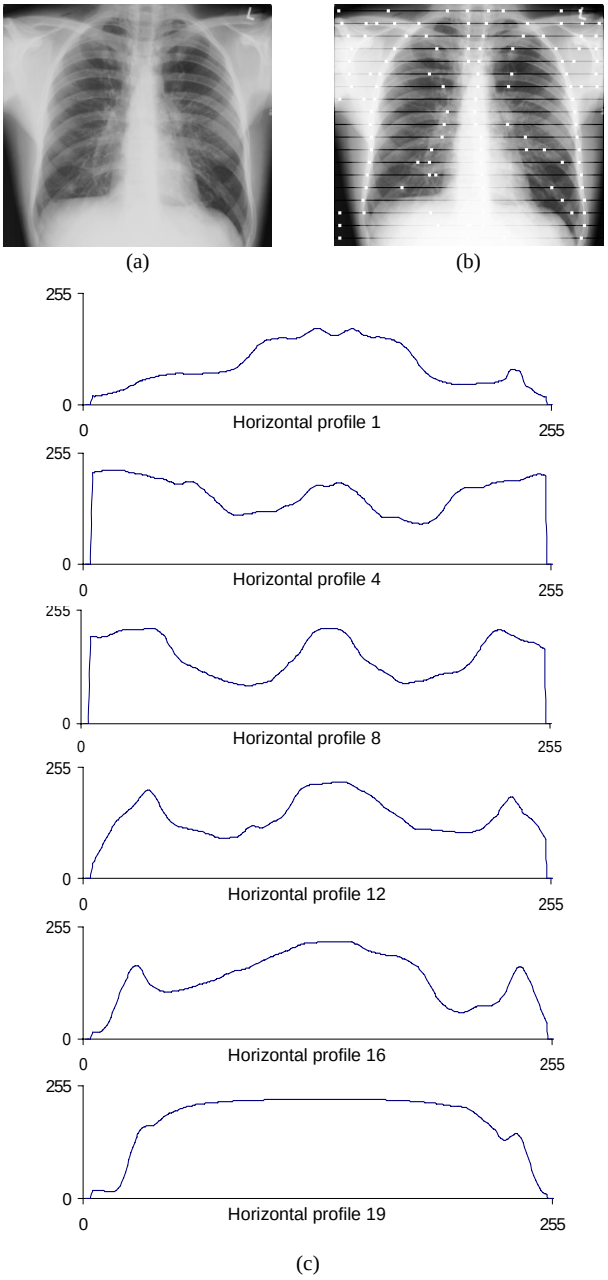

Fig. 1. Stationary chest radiograph from the IRMA dataset [19]. (a) Original image (serial no. 3166), (b) samples acquired and detected maxima, and (c) indicative profiles corresponding to the horizontal samples illustrated in Fig. 1(b).

The next step aims to select possibly relevant maxima and to classify them into three sets: a) spinal cord points, b) points of the left side of the ribcage, and c) points of the right side of the ribcage. To this direction, s_v non-overlapping rectangular windows of $N \times w$ pixels uniformly sample the radiograph from left to right, and the average intensity of each sample is estimated. Considering a stationary or a portable chest radiograph that displays both the patient's lungs, it is assumed that the spinal cord lies

roughly somewhere in the middle of the image. This is implemented by assigning as candidate spinal cord points the ones bilaterally closer to the column with the maximum average intensity within columns [M/4] and [3M/4]. This column will be referred to as the *central column C*.

Similarly, a *left column L* and a *right column R* are determined as the columns with the maximum average intensity between columns 0 and [M/4], and between columns [3M/4] and M, respectively. Considering the relative positions of the lung fields with respect to the spinal cord [7], the points closest to the left side of column [L+(C-L)/2] are selected as candidate points belonging to the left side of the ribcage and the points closest to the right side of column R+(R-C)/2 are selected as candidate points belonging to the right side of the ribcage.

The points assigned to the spinal cord are used by a *selective thresholding* algorithm to produce an auxiliary image for the detection of feature points defining the inner and bottom lung field boundaries.

Selective thresholding algorithm. This algorithm aims to remove the intensities of the radiograph that statistically characterize the anatomic structures between and under the lungs, leaving the intensities of the lung fields approximately unaffected. It is based on the fact that each structure is characterized by a set of intensities depicting its density, and that many of these structures such as the bones and the diaphragm extend beyond the spinal cord region. The algorithm proceeds as follows:

1. For each point i of the spinal cord:
   - 1.1 Acquire a sample of x^2 pixels;
   - 1.2 Calculate the intensity histogram h_i of each sample and select the histogram components around its highest peak;
   - 1.3 Accumulate the selected values from all samples into a single histogram H;
2. Find the last non-zero component m of H;
3. Generate a thresholded image $T(I)$ from I as follows:
   - Set the intensities of I that correspond to the non-zero components of H, to zero
   - Set the intensities of I that are larger than m, to zero.

The highest histogram peaks of a sample (step 1.2) correspond to the most representative grey-level intensities of that sample. This algorithm selects and removes only these intensities because part of the sample may contain intensities belonging to the lung fields. By acquiring samples from the whole spinal cord the most representative intensities of that region will be removed from the radiograph. It is worth noting that this algorithm removes also the heart and other structures of the mediastinum, since a significant part of them overlaps with the spinal cord. Consolidations that might be present in the lungs will remain almost unaffected as they are not likely to overlap with the spinal cord.

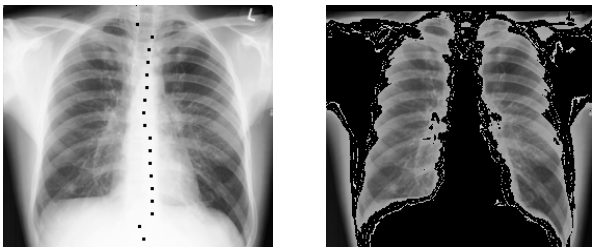

(a) (b)

Fig. 2. Selective thresholding. (a) Spinal cord points used in the sampling process, and (b) thresholded image $T(I)$.

The spinal cord points used in the sampling process as well as the output of the selective thresholding algorithm are illustrated in Fig. 2. It can be noticed that the interior of the lung fields remains almost intact.

2) Feature points of the inner lung field boundaries: Given a thresholded image $T(I)$, the inner lung field boundaries are likely to reside in the zero-intensity region of $T(I)$ between the points of the spinal cord and the first non-zero regions of $T(I)$ in the horizontal direction. Considering that the spinal cord region is typically characterized by the highest grey-level intensities in I, the inner lung field boundaries will be more or less identifiable by their edges. These edges will be less prevalent in the region of the heart and in regions of consolidation that may be present next to the inner lung field boundaries. Moreover, in some cases, especially if the quality of the radiograph is low (e.g. due to a low dynamic range), the possibility of discontinuities in the edges of the inner lung field boundaries cannot be eliminated.

In order to make inner lung field edges more prevalent, two directional edge maps are used, amplifying the left and right edges of I respectively. A map of vertical-left image edges $E_{vl}(I)$ and a map of vertical-right edges $E_{vr}(I)$ is obtained by convolution of I with the vertical-left 3×3 Sobel operator (having the negative signs on the left) and with the vertical-right 3×3 Sobel operator (having the negative signs on the right) [22].

The spinal cord points are linearly interpolated to form a continuous curve (the interpolation method is not critical at this step) and the feature points of the inner lung field boundaries are detected by the following algorithm:

1. For each point i of the spinal cord:
   Move left to find the point of $E_{vl}(I)$ with the maximum intensity for which $T(I)$ has zero intensity;
2. For each point i of the spinal cord:
   Move right to find the point of $E_{vr}(I)$ with the maximum intensity for which $T(I)$ has zero intensity.

The thresholded image $T(I)$ is used as a hard bound

protecting the feature point detection process from 'confusing' the inner lung field boundary edges with the strong vertical edges present within the lung fields.

This algorithm will produce many meaningful points over and under the lung fields, which will be filtered out during the parametric curve approximation process.

Another important aspect of this algorithm is that the points detected lie at the inner edges of the lung fields even in the region overlapped by the heart. Consequently, the lung field boundaries approximated by the proposed methodology will include this heart region, behind which consolidations due to bacterial pulmonary infections can be found [2]. This is an additional feature of the proposed methodology over the current ones, which systematically exclude the overlapping heart region from the lung fields [1]-[13],[18].

3) Feature points of the bottom lung field boundaries: A similar approach can be applied for the detection of feature points at the bottom lung field boundaries. The application of the selective thresholding algorithm on I can lead to an image $T(I)$ having most grey-level intensities below the diaphragms set to zero. Convolving I with the horizontal 3×3 Sobel operator [22] a horizontal edge map $E_h(I)$ is obtained. The algorithm for the detection of the bottom lung field boundaries proceeds as follows:

1. For each column of I between the leftmost point of the left boundary and the rightmost point of the right boundary

   Begin from row M-1 to find the point of $E_h(I)$ with the maximum intensity for which $T(I)$ has zero intensity.

As with the previous algorithm, many of the points falling beyond the lung fields may be meaningful; however, these will be filtered out during the parametric curve approximation process.

B. Removal of outliers

Many of the feature points detected with the algorithms described in the previous subsection (Fig. 3a), are outliers which have to be filtered out so as to obtain a smoother and more accurate approximation of the lung fields.

In order to purify the feature points of the outer left and right lung field from possible outliers, the grey-level intensity of each point is compared with the average intensity of the set of points assigned to the corresponding boundary. Only the points with grey-level intensities approximating the average are selected as valid. The rest are discarded based on the fact that the densities of the spinal cord and the densities of the ribcage do not vary significantly across the perpendicular axis of a radiograph.

Similarly, outliers may reside within the points assigned to the inner and the bottom lung field boundaries detected. Correspondingly, a point is considered as an outlier if its horizontal or vertical position deviates from the average position of its k nearest neighbors.

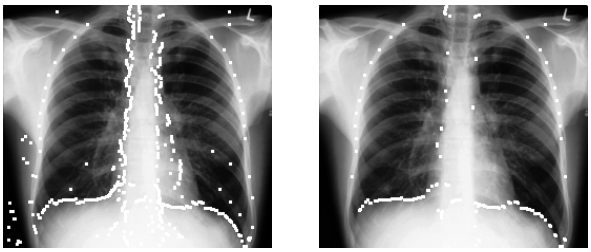

(a) (b)

Fig. 3. Feature points detected. (a) All points, (b) points remaining after removal of outliers.

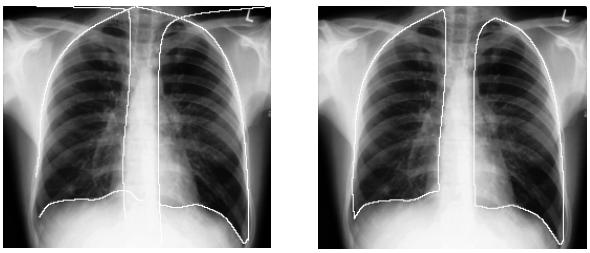

(a) (b)

Fig. 4. Lung field detection obtained using the proposed methodology: (a) before and (b) after discarding and connecting curve segments.

The detected feature points after removal of outliers are illustrated in Fig. 3(b).

C. Parametric curve approximation

The feature points detected for each boundary are then interpolated using Bézier curves [21]. The Bézier curves are intuitively manipulated via a set the control points, in the sense that the curve is attracted by the internal control points without necessarily passing through them. This feature provides tolerance to the presence of outliers that may be remaining in the control points, and leads to smoother approximation of the lung field boundaries as compared with other interpolation approaches.

Let P_0, P_1, …,P_n, be feature points detected for a lung field boundary. The boundary is then approximated according to equation

$$B(t) = \sum_{i=0}^{n} \binom{n}{i} P_i (1-t)^{n-i} t^i \qquad (1)$$

where $t \in [0,1]$.

Each lung field is approximated by three Bézier curves. The points beyond the intersection of each pair of the three curves are discarded. If the ending points are not intersecting they are extended so that they connect to each other. As a result, each lung field is approximated by three consecutive curves (Fig. 4).

III. Results

The proposed methodology was evaluated with two sets of experiments. The first set, investigates its performance on various stationary radiographs obtained from a standard database, and a second set investigates its performance on a

harder set of portable radiographs.

All radiographs used in the experiments have been digitized at 8 bits and have been downscaled to fit a 256×256-pixel bounding box. The parameters used are: sampling windows of $w=h$, where $8 \le h \le 24$, for local maxima estimation; sampling windows of $x=32$ for selective thresholding, and $k=5$ neighbors for outlier removal.

The accuracy of the proposed methodology was quantified by the overlap between the automatically detected area a and a ground truth area g indicated by an expert [23]:

$$accuracy = \frac{a \cap g}{a \cup g} \quad (2)$$

The image processing algorithms used, as well as the algorithms presented in this study have been implemented in Java to take advantage of its cross-platform compatibility and the language's ability to facilitate modular design.

A. Stationary radiographs

The stationary chest radiographs used for this set of experiments have been selected from the IRMA (Image Retrieval in Medical Applications) dataset. This dataset is often used as a reference for medical image retrieval tasks and contains arbitrarily selected anonymous radiographic images taken randomly from patients of different ages, genders and pathologies during medical routine. For the purposes of this study a random subset of 24 chest radiographs was selected. Radiographs in which the lung fields are partially absent have not been included in this subset.

Provided that the appropriate parameters are set for each of the available radiographs the average accuracy achieved is approx. 98.4%. However, as fully automatic operation requires constant parameter settings, the average accuracy was measured for various values of h as illustrated in Fig. 5. The best average approximation accuracy achieved is 95.6% with $h=10$. Indicative output images obtained with this setting are illustrated in Fig. 4(b) and in Fig. 6.

B. Portable radiographs

Twenty four anonymous portable radiographs obtained from patients with bacterial pulmonary infections have been provided for the purposes of this study by the Chest Hospital of Athens "Sotiria" in the context of the European project DEBUGIT [24]. This dataset is quite challenging as in all radiographs the lung fields appear misaligned and distorted, they include consolidations "hiding" their boundaries, and contain dense external objects used for patients' monitoring.

The average accuracy measured using near-optimal settings for each radiograph reached 93.2%. The average accuracies measured for common values of h for all the available portable radiographs are illustrated in Fig. 7. The best average approximation accuracy achieved is 90.8% with $h=9$. An indicative output image obtained with this setting is illustrated in Fig. 8. It can be noticed that the approximation obtained is quite accurate although the original radiograph exhibits severe consolidations on the right lung field. The proposed methodology managed to detect the lung field boundaries without getting affected by the strong edges of the dark formation that corresponds to a non-consolidated area in the right lung field. Another important observation is that the region of the heart overlapping the lung fields has been included in the delineated region. Slight deviations from the correct boundaries can be observed only at the top of the right lung field where an external object attracted the curve, and at the bottom of the left lung field which is partially visible. Similar observations are valid for the rest of the dataset.

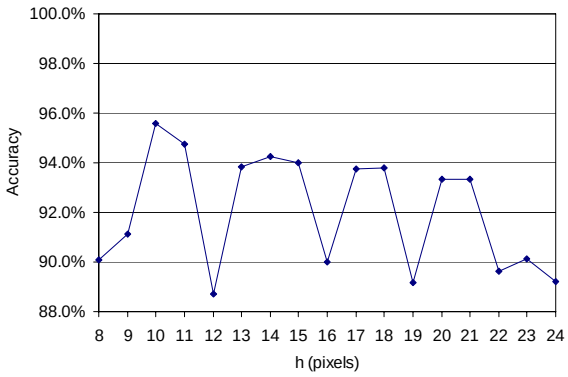

Fig. 5. Average lung field approximation accuracy obtained by the application of the proposed methodology on stationary radiographs using sampling windows of various heights h.

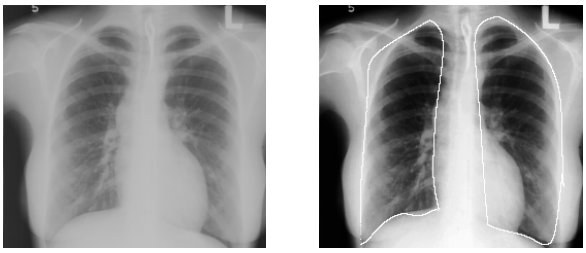

(a) (b)

Fig. 6. Indicative results on another radiograph from the IRMA dataset [19]. (a) Original image (serial no. 3180), and (b) output images with detected lung fields.

IV. Conclusions and Future Work

This study presented a novel approach to lung field detection and boundary approximation in the presence of bacterial pulmonary infections, based on statistical grey-level intensity information and directional edge maps. The initial results from its application on various stationary chest radiographs showed that its accuracy can be comparable to the accuracy of more complex state of the art methodologies without being dependent on some training data set [13].

More importantly, the results from its application on portable chest radiographs validate its suitability for the analysis of portable radiographs, which is a challenging new area of research.

In summary, the proposed methodology has the following features:

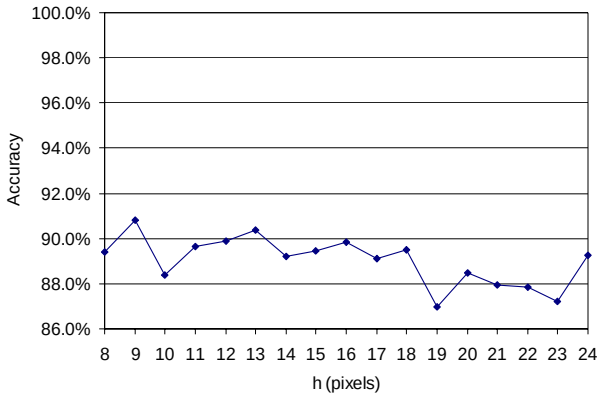

Fig. 7. Average lung field approximation accuracy obtained by the application of the proposed methodology on portable radiographs using sampling windows of various heights *h*.

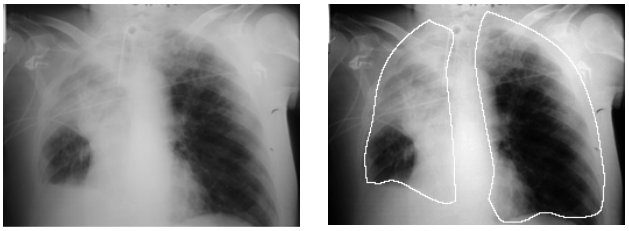

(a) (b)

Fig. 8. Indicative results from the application of the proposed methodology on a portable radiograph with pulmonary infection. (a) Original image. (b) Output image with detected lung fields.

1) it is versatile, well-functioning on both stationary and portable chest radiographs, since it is not limited by the patient's positioning.
2) it is tolerant to the presence of consolidations and boundary discontinuities of the lung fields.
3) it is unsupervised, in the sense that it does not require training;
4) it does not exclude the region of the lung fields overlapped by the heart from its output, as current methodologies do, enabling the detection of abnormalities even behind the heart.

Future work includes further experimentation with larger datasets and improvement of the robustness of the proposed methodology against factors affecting its accuracy. Such factors include the presence of objects used for the patient's monitoring, and the absence of parts of the lung fields from the radiograph. The perspectives of this study extend to a broad spectrum of applications in computerized analysis of chest radiographs with special focus on robust automatic assessment of pulmonary infections

ACKNOWLEDGMENTS

Great thanks to Mr. G. Papamichalis, M.D. who generously offered his help and advice on the medical aspects of this study. Part of the radiographs used is courtesy of Dr. T.M. Lehmann, Image Retrieval in Medical Application (IRMA) group, Dept. of Medical Informatics, RWTH Aachen, Germany, http://irma-project.org.

REFERENCES

[1] P.H. Meyers, H.C. Nice, C.M. Becker, N.J. Nettleton, J.W. Sweeney, and G.R. Meckstroht, "Automated Computer Analysis of Radiolographic Images," *Radiology*, vol. 13, pp. 1029-1034, 1964.
[2] N.L. Müller, T. Franquet, K.S. Lee, C. Isabela, and S. Silva, *Imaging of Pulmonary Infections*, Lippincott Williams & Wilkins, 2006
[3] F.S. Bongard, and D.Y. Sue, *Current Critical Care Diagnosis & Treatment*, 2nd ed., McGraw-Hill/Appleton & Lange, 2002
[4] B.V. Ginneken, B.T.H. Romeny, and M.A. Viergever, "Computer-Aided Diagnosis in Chest Radiography: A Survey," *IEEE Trans. Medical Imaging*, vol. 20, no. 12, pp. 1228-1241, Dec. 2001.
[5] B.V. Ginneken, S. Katsuragawa, B.T.H. Romeny, K. Doi, and M.A. Viergever, "Automatic Detection of Abnormalities in Chest Radiographs Using Local Texture Analysis," *IEEE Trans. Medical Imaging*, vol. 21, no. 2, pp. 139-149, Feb. 2002.
[6] J. Duryea, and J. Boone, "A Fully Automatic Algorithm for the Segmentation of Lung Fields in Digital Chest Radiographic Images," Medical Physics, vol. 22, no. 2, pp. 183-191, 1995
[7] X.-W. Xu, and K. Doi, "Image Feature Analysis for Computer Aided Diagnosis: Accurate Determination of the Ribcage Boundary in Chest Radiographs," Medical Physics, vol. 22, no. 5, pp. 617-626, 1995.
[8] H. Luo, R. Gaborski, R. Acharya, "Automatic Segmentation of Lung Regions in Chest Radiographs: A Model Guided Approach," in *Proc. Int. Conf. Image Processing (ICIP 2000)*, vol. 2, 2000, pp. 483-486.
[9] B.V. Ginneken, and B.T.H. Romeny, "Automatic Segmentation of Lung Fields in Chest Radiographs," *Medical Physics*, vol. 27, no. 10, pp. 2445-2455, 2000.
[10] I. Iglesias, P.G. Tahoces, M. Souto, A. Martinez de Alegria, M.J. Lado, and J.J. Vidal, "Lung Segmentation on Postero-anterior Digital Chest Radiographs Using Active Contours," *Lecture Notes in Computer Science*, vol. 3138, pp. 538-546, 2004.
[11] G. Coppini, S. Diciotti, M. Falchini, N. Villari, and G. Valli, "Neural Networks for Computer-Aided Diagnosis: Detection of Lung Nodules in Chest Radiograms," IEEE Trans. on Information Technology in Biomedicine, vol. 7, no. 4, pp. 344-357, Apr. 2003.
[12] N. Vittitoe, R. Vargas-Voracek, and C. Floyd Jr, "Markov Random Field Modeling in Posteroanterior Chest Radiograph Segmentation," Medical Physics, vol 26, no. 8, pp. 1670-1677, 1999.
[13] B.V. Ginneken, M.B. Stegmann, M. Loog, "Segmentation of Anatomical Structures in Chest Radiographs using Supervised Methods: A Comparative Study on a Public Database," *Medical Image Analysis*, vol. 10, pp. 19-40, 2006.
[14] T. Cootes, C. Taylor, D. Cooper, and J. Graham, "Active Shape Models - Their Training and Application," *Computer Vision and Image Understanding*, vol 61, no. 1, pp. 38-59, 1995.
[15] X. Xie, X. Li, S. Wan, and Y. Gong, "Mining X-Ray Images of SARS Patients," in G.J. Williams and S.J. Simoff (Eds.) Data Mining, Lecture Notes in Artificial Intelligence, vol. 3755, pp. 282-294, 2006.
[16] J. Liang, T. McInerney, and D. Terzopoulos, "United Snakes. *Medical Image Analysis*, vol. 10, pp. 215-233, 2006.
[17] T. Yu, J. Luo, N. Ahuja, "Shape Regularized Active Contour using Iterative Global Search and Local Optimization," in *Proc. Comp. Vis. Pat. Rec. Conf. (CVPR 2005)*, vol.2, pp. 655- 662, 2005.
[18] S. Chen, L. Cao, J. Liu, X. Tang, "Automatic Segmentation of Lung Fields from Radiographic Images of SARS Patients Using a New Graph Cuts Algorithm," in *Proc. Int. Conf. Pat. Rec. (ICPR 2006)*, vol. 1, pp. 271-274, 2006.
[19] T.M. Lehmann, M.O. Güld, C. Thies, B. Plodowski, D. Keysers, B. Ott, H. Schubert, "IRMA - Content-based image retrieval in medical applications," in *Proc. 14th World Congress on Medical Informatics (Medinfo)*, IOS Press, Amsterdam, vol. 2, pp. 842-848, 2004.
[20] Novelline, R.A. (1997) *Squires's Fundamentals of Radiology*. Cambridge: Harvard University Press.
[21] R.H. Bartels, J.C. Beatty, and B.A. Barsky, Bézier Curves. Ch. 10 in *An Introduction to Splines for Use in Computer Graphics and Geometric Modelling*. San Francisco, CA: Morgan Kaufmann, pp. 211-245, 1998.
[22] R.C. Gonzalez, and R.E. Woods, *Digital Image Processing*, 3rd ed., Prentice Hall, Upper Saddle River, NJ, 2008.
[23] D.K. Iakovidis, M.A. Savelonas, S.A. Karkanis, D.E. Maroulis, "A Genetically Optimized Level Set Approach to Segmentation of Thyroid Ulrtrasound Images," *Applied Intelligence*, vol. 27, no. 3, pp.193-203, 2007.
[24] C. Lovis, D. Colaert, V.N. Stroetmann, "DebugIT for Patient Safety - Improving the Treatment with Antibiotics through Multimedia Data Mining of Heterogeneous Clinical Data," *Stud Health Technol. Inform.*, vol. 136, 641-646, 2008.